PHYSICAL REVIEW B **82**, 125314 (2010)

Ultrafast few-fermion optoelectronics in a single self-assembled InGaAs/GaAs quantum dot

M. Zecherle* and C. Ruppert
Physik Department E11, TU München, James-Franck-Str, 85748 Garching, Germany

E. C. Clark, G. Abstreiter, and J. J. Finley
Walter-Schottky-Institut and Physik Department E24, TU München, Am Coulombwall 3, 85748 Garching, Germany

M. Betz
Physik Department E11, TU München, James-Franck-Str, 85748 Garching, Germany and Experimentelle Physik 2, TU Dortmund, 44221 Dortmund, Germany

(Received 22 June 2010; published 14 September 2010)

We report a comprehensive study of the ultrafast optoelectronic response of a single self-assembled InGaAs/GaAs quantum dot embedded in a *n-i*-Schottky photodiode device. While manipulation of the artificial atom relies on two independently tunable picosecond pulse trains, sensitive all electrical readout is achieved via photocurrent. We apply our methods to probe the temporal evolution of the quantum dot absorption spectrum following coherent optical generation of a *s*-shell exciton. Our measurements reveal the biexciton absorption as well as previously unobserved *p*-shell transitions that appear in the presence of *s*-shell population. Furthermore, time-resolved measurements allow us to directly monitor the picosecond tunneling times of electrons and holes out of the dot. Beyond these incoherent phenomena, we also demonstrate the potential of our techniques for coherent quantum dot manipulations. Beginning with excitonic Rabi oscillations driven by a single pulse tuned to the neutral exciton we move on to demonstrate the coherent generation of the biexciton via a two-photon nonlinearity, before realizing conditional Rabi oscillations in the exciton-biexciton state manifold. The results provide significant potential for realizing and utilizing conditional coherent dynamics in quantum dot nanostructures for all optical, ultrafast quantum information processing.

DOI: 10.1103/PhysRevB.82.125314 PACS number(s): 78.67.Hc, 78.47.D−, 03.67.Lx, 42.50.Hz

I. INTRODUCTION

The three-dimensional quantum confinement in semiconductor quantum dots (QDs) leads to a number of remarkable optical properties of these "artificial atoms."[1,2] Novel applications such as single-photon emitters and nonclassical current sources have already been demonstrated[3] and some applications, such as high-power laser diodes,[4] are by now well established.[5] Spin and charge degrees of freedom of individual QD nanostructures are promising candidates for all optical solid-state quantum information processing. One possible realization is to encode the qubit in an excitonic basis; the qubit being defined by logical states corresponding to the presence or absence of an exciton in the dot.[6] This approach calls for the manipulation of a single QD via a sequence of independently tunable picosecond laser pulses to address the quantum states of the system. Considerable progress has been made toward the coherent optical control of a single exciton qubit.[7–11] However, the realization of a quantum processor requires the development of systems having a conditional coherent response. Two-qubit gates were first demonstrated in GaAs interfacial QDs (Ref. 12) that typically suffer from shallow confinement and short dephasing times. Recently, a gate was realized by selectively driving exciton-biexciton transitions in a single self-assembled InGaAs QD embedded in a Schottky photodiode.[13] Further progress and scaling toward a larger number of qubits calls for addressing of excited excitons involving higher orbital states (*p* and *d* shells) of the QD. With this goal in mind, it is essential to understand how the interband optical response of a single dot is modified following excitation.

In this paper, we report on ultrafast spectroscopic experiments on individual self-assembled InGaAs/GaAs quantum dots subject to ultrafast optical excitation. The dots are embedded within a *n-i*-Schottky photodiode to allow sensitive electrical readout via photocurrent. The study utilizes two independently tunable trains of picosecond pulses allowing us to perform pump-probe measurements on a single dot with sub-10 ps temporal resolution. The results obtained provide insight into the nonlinear optical response over a much broader spectral range than has been possible previously.[13,14] The paper is organized as follows: following the Sec. I, Sec. II describes the samples used for our studies and the experimental setup developed to deliver two time-delayed picosecond excitation pulses to the device. Section III is devoted to pump-probe-type experiments, whereby the modification of the QDs absorption spectrum of the dot, and its evolution with time is monitored after coherent preparation of a neutral exciton. Following excitation, we clearly observe the emergence of the biexciton transition and, most remarkably, the wide spectral range provided by our approach allows us to observe the excited state (*p*-shell) transitions, perturbed by the presence of a *s*-shell exciton. We show that the presence of the exciton leads to millielectron volt energy shifts of the excited-state interband transitions. The dynamics of the QD occupation is analyzed in Sec. IV where we directly monitor the tunneling times of both electrons and holes out of the QDs *s*-shell in the time domain. Section V discusses strong excitation phenomena. In addition to the well-known excitonic Rabi flip,[8] we directly observe optical gain at the excitonic ground-state transition, monitor its temporal dynamics

and demonstrate the possibility of direct single-pulse biexciton generation via a two photon nonlinearity. Finally, in Sec. VI we demonstrate conditional Rabi oscillations of the exciton-biexciton transition following coherent excitation of the exciton.[13] In this regime, the QD photodiode acts as a deterministic current source, delivering precisely two elementary charges per excitation cycle. In order to facilitate direct comparison, all the results presented were obtained from the same QD. We summarize our results and conclusions in Sec. VII.

II. SAMPLE STRUCTURE AND EXPERIMENTAL SETUP

The InGaAs/GaAs QDs studied here were grown with standard self-assembly techniques.[1] To allow for photocurrent experiments, the InGaAs QDs are embedded at the midpoint of a 400-nm-wide intrinsic region of a GaAs *n-i*-Schottky diode structure with a semitransparent titanium top contact. To isolate individual quantum dots, growth conditions were employed that provided an areal density of a few QDs per square micron. By defining opaque gold shadow masks on the sample surface single dots could be reproducibly addressed. Such shadow masks are fabricated by depositing 1-μm-diameter polystyrene microspheres on the wafer prior to the deposition of an optically opaque 200-nm-thick gold layer. Subsequent removal of those spheres produces circular micron-sized apertures which enable us to reproducibly address a single QD. A voltage applied to the top gate with respect to a buried *n*+ doped contact results in an electric field within the intrinsic region and allows us to switch between two regimes in which the dominant relaxation mechanism of carriers localized in the QD proceeds by (i) optical recombination or (ii) tunneling. For small electric fields (<20 kV cm^{-1}) and low temperatures, optical recombination dominates the relaxation of an occupied QD. In contrast, for large backward voltages the electric field becomes larger and tunneling out of the QD occurs over time scales that are much faster than the radiative decay. For the purposes of this study, we operated in the latter photocurrent regime[15] where most carriers generated by interband transitions tunnel out of the dot over a controlled time scale, thus contributing to a current in the external circuit. For the majority of our experiments the diode structure is biased with $V_B=-750$ mV which gives rise to an internal electric field of 37 kV/cm.

The probe-induced current, in turn, is a direct measure of the absorption response of the dot. For all measurements the sample is held in a microscope cryostat at a constant temperature of 10 K.

Ultrafast pump-probe-type experiments require two independently tunable, time-delayed picosecond laser pulse trains. The experimental scheme is similar to the one reported by Boyle *et al.*[13] and is depicted in Fig. 1. However, the starting point here is a mode-locked Ti:sapphire laser ($f_{\mathrm{rep}}=60$ MHz) delivering broadband, ≈ 40 fs pulses at 910 nm.[16] As a result, the bandwidth is sufficient to cover almost the entire spectral window from the excitonic ground state of the QD to the wetting layer band edge. The laser output is split to form pump and probe pulse trains. Each pulse train

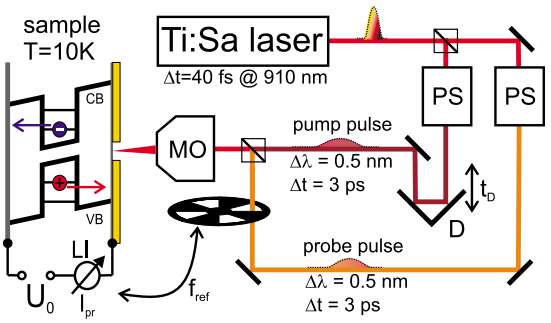

FIG. 1. (Color online) Schematic of the experimental setup: picosecond pump and probe pulses are spectrally sliced out of a broadband femtosecond laser using two 4f-PS. The time delay t_D between the pulses is adjusted via a motorized D. A MO focuses the two pulse trains on a micron shadow mask on the sample mounted in a microscope cryostat. The sample is electrically biased and the probe-induced photocurrent is analyzed by a LI.

passes through an independent 4f-pulse shaper.[17] A slit positioned on a motorized stage slices spectrally narrow pulses out of the broadband input (spectral width of ≈ 0.7 meV). A small spatial separation of the slit and the Fourier plane of the pulse shaper (PS) ensures a smooth spectrum and thereby avoids satellite pulses in the time domain. The pulses are practically bandwidth limited and provide a time resolution of ≈ 3 ps for our pump-probe studies. Pump and probe pulses are superimposed collinearly and focused into the microscope cryostat using a reflective mirror objective (MO) (NA=0.4). Typical excitation spot sizes are measured to be ≈ 2 μm. The time delay t_D between pump and probe pulse is controlled via a motorized delay stage (D) in the probe beam. This setup allows us to vary the delay in the range from -300 to $+500$ ps with a precision better than 5 fs.

The train of probe pulses (photon energy E_{Pr}) is mechanically chopped at a frequency $f_{\mathrm{ref}}=470$ Hz. A Stanford SR830 digital lock-in amplifier (LI) is referenced to f_{ref} to extract the probe-induced photocurrent $I_{\mathrm{Pr}}(E_{\mathrm{Pr}})$ through its very sensitive (10^8 V A^{-1}) current input. In most experimental situations $I_{\mathrm{Pr}}(E_{\mathrm{Pr}})$ directly reflects the QD absorption spectrum.[18,19] Upon blocking the pump beam the absorption spectrum $I_{\mathrm{Pr}}^{(0)}(E_{\mathrm{Pr}})$ of the QD is measured with the dot initially in its crystal ground state. Unblocking the pump beam the measurement is then repeated to detect the QDs absorption spectrum $I_{\mathrm{Pr}}(t_D,E_{\mathrm{Pr}})$ at a time t_D after the interaction with the pump pulse. The pump triggered change in probe-induced photocurrent $\Delta I_{\mathrm{Pr}}(t_D,E_{\mathrm{Pr}})=I_{\mathrm{Pr}}(t_D,E_{\mathrm{Pr}})-I_{\mathrm{Pr}}^{(0)}(E_{\mathrm{Pr}})$ is then calculated by subtraction of the two signals. A variation in E_{Pr} and t_D therefore provides comprehensive insight into the time-dependent optical properties of the QD after excitation. We note that in $I_{\mathrm{Pr}}(E_{\mathrm{Pr}})$ spectra the spectrally narrow peaks of the QD absorption lines are typically accompanied by a spectrally unstructured background[20] that increases linearly with the incident laser power. The origin of this background most likely is related to light that enters the shadow mask and is absorbed by other QDs in the same diode structure.[21] For clarity, in all the measurements presented in this paper this background has been subtracted from the data.

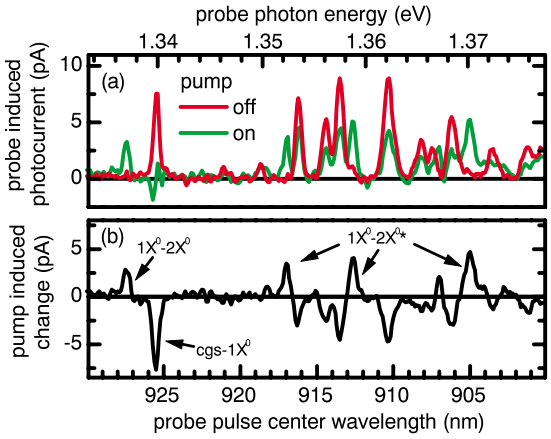

FIG. 2. (Color online) (a) Pump off: photocurrent spectrum as detected with the probe pulse only. Pump on: photocurrent spectrum detected $t_D=3$ ps after exciting the cgs$\rightarrow$X^0 transition. (b) Difference of the two photocurrent spectra with same abscissa scaling. Positive (negative) signals indicate pump-induced bleaching (absorption). The arrows indicate the excitonic transitions discussed in the main text.

III. MODIFICATION OF THE QUANTUM DOT ABSORPTION BY SELECTIVE *s*-SHELL OCCUPATION

In a first set of experiments we focus on pump-probe-type experiments in order to monitor the change in the QDs absorption spectrum and its temporal evolution following selective resonant excitation of the ground-state exciton transition. First the pump beam is blocked and the sample is illuminated by the probe pulse train only. Scanning the photon energy E_{Pr} of the narrow band ($\Delta E_{\mathrm{Pr}}=0.7$ meV) probe pulse train over a broad spectral range, an absorption spectrum of the QD is obtained. We note that due to the limited spectral width of the laser source, the probe intensity changes by a factor of two over the spectral range from 1.335 to 1.375 eV and the data are not corrected for this variation. In the spectral range of the *s* shell of the QD transition the incident probe pulse energy on the geometrical area of the shadow mask aperture is 1.8 fJ, which is about 80% of the energy of a π pulse as determined in Sec. V. of this paper. The observed photocurrent spectrum [cf. Fig. 2(a)] consists of a series of sharp absorption peaks with a width limited by the spectral width of the probe pulse. The isolated peak at $E_{\mathrm{Pr}}=1.3399$ eV corresponds to the transition from the empty dot in the crystal ground state (cgs) to the single exciton (X^0) in its *s*-shell orbital state. The other peaks at higher photon energy are spectroscopic signatures of excited excitons in *p*- and *d*-shell states. The overall magnitude of the photocurrent is as large as 8 pA when exciting an excitonic resonance. This value is close to the theoretical maximum of $I=e\cdot f_{\mathrm{rep}}=9.3$ pA which corresponds to a current of one elementary charge per excitation cycle. This finding points toward efficient carrier extraction from the quantum dot and probe areas close to a π pulse.

In the next step, the pump pulse is precisely tuned into resonance with the cgs$\rightarrow$X^0 transition and the delay time between pump and probe pulses is fixed at $t_D=3$ ps, i.e., much shorter than typical tunneling times of electrons or holes out of the dot ($\approx$100 ps, see Sec. IV). The incident pump power is 1.1 fJ per pulse. Repeating the spectral scan reveals an entirely different absorption spectrum [cf. Fig. 2(a)]. Most strikingly, for this specific pump intensity the absorption peak corresponding to the generation of a *s*-shell exciton is almost entirely suppressed. To facilitate the further analysis we calculated the difference $\Delta I_{\mathrm{Pr}}(t_D,E_{\mathrm{Pr}})$ of the two absorption spectra. The results of this procedure are presented in Fig. 2(b). In this representation, negative signals indicate bleaching of a transition while positive signals correspond to a pump-induced absorption. Remarkably, bleaching is observed for all the transitions of the empty QD [red line in Fig. 2(a)] providing strong evidence that all of these spectral signatures belong to the same QD. This evidence is intrinsically difficult to extract by employing other spectroscopic methods such as luminescence or CW photocurrent spectroscopy.

We now turn toward the discussion of the induced absorption signals in Fig. 2(b). In an occupied dot, the probe pulse can, in general, add another electron-hole pair in the *s* shell of the dot to form a biexciton (2X^0). Due to the Coulomb interaction and correlation effects the X$^0\rightarrow$2X^0 transition is spectrally detuned from the cgs$\rightarrow$X^0 transition by an energy of few millielectron volt.[22–24] In Fig. 2(b), such an induced biexcitonic absorption is clearly observed at a probe photon energy of $E_{\mathrm{Pr}}=1.3370$ eV. As a result, we can directly infer a biexciton binding energy of 2.9 ± 0.3 meV.

At larger photon energies $E_{\mathrm{Pr}}>1.35$ eV peaks of pump-induced absorption are observed in addition to the biexciton transition discussed above. These features arise from excited biexciton transitions whereby one electron-hole pair resides in the *s*-shell and the probe pulse generates another in excited states. These electronic configurations of the QD are inaccessible using, e.g., photoluminescence experiments because relaxation of carriers to the *s* shell is significantly faster than optical recombination. Therefore while theoretically predicted as intermediate states in the decay of multiexciton complexes[25] these states have not been previously observed directly. The absorption line signatures of those excited biexciton states are found energetically close to *p*- or *d*-shell transitions observed when exciting an empty dot. Interestingly, the energy differences which correspond to biexcitonic binding energies are seen to be both negative (line pair at 1.352 eV, Fig. 2) and positive (line pair at 1.358 eV, Fig. 2), reflecting the delicate interplay of attractive and repulsive Coulomb correlations in the excited four-particle state. The Coulomb renormalization energies for excited biexcitons tend to be smaller than the value of 2.9 ± 0.3 meV of the *s*-shell biexciton, indicating that the motional correlation effects are weaker for the excited biexciton states. Further quantitative analysis of these renormalization energies can only be performed by comparing our findings with detailed theoretical calculations. Thus, we restict our discussion here to the observation of excited biexciton states without delving deeper into the quantitative aspects.

From the complete bleaching of the pumped cgs$\rightarrow$X^0 transitions, it follows that the pump-induced (statistical) occupation of the X^0 state is very close to 50% at the time of the arrival of the probe pulse. In the other 50% of the cases

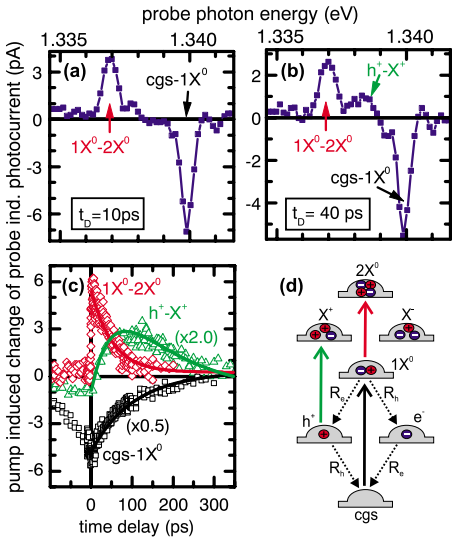

FIG. 3. (Color online) *s*-shell population dynamics: pump-triggered changes in the probe-induced photocurrent for various delay times after resonant excitation of the cgs$\rightarrow$X^0 transition. [(a) and (b)] Spectral scans at different time delays. (c) Temporal scans at the fixed photon energies in resonance with the transitions labeled in the spectra. For better visibility the signal amplitudes have been rescaled by the factors given in the graph. Solid lines represent the result of a fit with a rate-equation model introduced in the main text. (d) Schematic level diagram visualizing the probed optical transitions (arrows pointing upwards) and the tunneling rates R_e and R_h used in the rate equation model for the decay of the X^0 population.

the QD remains in the cgs. Also the $\approx$50% bleaching of the absorption peaks at higher probe intensity (see peaks at E_{Pr}=1.3575 eV or E_{Pr}=1.3622 eV, Fig. 2) strongly supports this interpretation since here the final state of the probed transition is empty and not populated by the preceding pump pulse. The amplitude photocurrent of the induced X^0-2X^0 absorption is 3.2 pA, which is close to 50% of the signal amplitude at the cgs-X^0 transition measured without pump pulse. These observations indicate that the oscillator strengths of biexciton and neutral exciton transitions are comparable. From this type of measurement and results presented in the following sections, we estimate that the ratio of oscillator strength of the X$^0\rightarrow$2X^0 transition to the cgs$\rightarrow$X^0 transition is in the range from 1.0 to 1.15.

IV. DYNAMICS OF ELECTRON AND HOLE TUNNELING

In this section, we shift our attention to the time-resolved analysis of the QDs occupation. In particular, the observation in Fig. 2 of both a bleaching signal of the cgs$\rightarrow$X^0 transition and the induced absorption at the biexciton resonance strongly indicate that the QD is populated by a single electron-hole pair. Thus, performing measurements in the time domain provide direct information on the temporal evolution of the QD population. The concept is readily understood from the data presented in Fig. 3 that show the modifications of the probe-induced photocurrent after pumping the cgs$\rightarrow$X^0 transition for three different transitions. Upon probing the X$^0\rightarrow$2X^0 absorption [circles in Fig. 3(c)], the signal sharply increases at t_D=0 and decays over a time scale of shorter than 100 ps. For the case when the probe pulse is tuned to the cgs$\rightarrow$X^0 resonance (squares) and $t_D>0$, a similar bleaching trace of opposite sign is found. The signal at negative delay times reflects the indistinguishability of pump- and probe-induced changes in the total photocurrent in this degenerate configuration where pump and probe pulses both excite the cgs$\rightarrow$X^0 transition. In particular, for similar powers of pump and probe pulses the signal would be expected to be symmetric around t_D=0. The decay times of all these signals direct evidence for a QD depopulation that is governed by carrier tunneling of the confined QD states, thereby restoring the cgs.

In order to make a quantitative analysis of this tunneling spectral scans at different t_D were measured. Examples of such spectra are depicted in Figs. 3(a) and 3(b). They allow us to identify a weak induced absorption at probe photon energies of E_{Pr}=1.3384 eV. This absorption line is present neither for $t_D\leq 0$ nor in measurements without pump pulse. A temporal scan [triangles in Fig. 3(c)] at this probe photon energy demonstrates that the amplitude of this absorption rises in parallel with the decay of the other signal amplitudes and then decays on a slower time scale of more than 100 ps. We attribute this absorption to the intermediate state that appears in the sequential tunneling process which, due to the lighter electron mass, is most likely the QD occupied with the photogenerated hole (h$^+$). Thus, following the excitation of the system with the pump pulse a transient absorption (h$^+\rightarrow$X$^+$) appears after the electron has tunneled out of the dot, that persists until the hole tunnels out. This feature provides direct information on the carrier tunneling escape of both electron and hole from the system. We note that the spectral position of the h$^+\rightarrow$X^0 transition indicates this complex to be bound relative to the neutral exciton X^0. However, this finding is probably specific to the details of the investigated QD as well as to the bias voltage to the device and might not apply to InGaAs QDs in other experimental configurations.

We analyze these findings with a simple rate equation model illustrated by Fig. 3(d). At t_D=0 ps, the pump pulse generates the initial occupations $N_{1\mathrm{X}}(t=0)=N_0$ of the X^0 state and $N_{\mathrm{cgs}}(t=0)=1-N_0$ of the cgs. Subsequently, electrons and holes tunnel out of the QD with independent rates R_e and R_h, respectively. The analytic solutions of the rate equations for these starting parameters are

$$N_{1\mathrm{X}}(t) = N_0 \exp[-(R_e+R_h)t], \tag{1}$$

$$N_h(t) = N_0\{-\exp[-(R_e+R_h)t]+\exp(-R_e t)\}, \tag{2}$$

$$N_e(t) = N_0\{-\exp[-(R_e+R_h)t]+\exp(-R_h t)\}, \tag{3}$$

$$N_{\mathrm{cgs}}(t) = 1 - N_{1\mathrm{X}}(t) - N_h(t) - N_e(t). \tag{4}$$

Here N_e and N_h are the populations of the intermediate states with only one electron or one hole in the QD. Probing an optical transition results in a probe-induced photocurrent with an amplitude that is proportional to the difference of the occupations of the final state and the initial state. Since the

final states of the $h^+ \rightarrow X^+$ and $X^0 \rightarrow 2X^0$ transitions are not occupied before probing, the number of the positively charged QDs (N_h) and the X^0 population (N_{1X}) can be directly compared to the temporal scans probing the $h^+ \rightarrow X^+$ and the $X^0 \rightarrow 2X^0$ transitions, respectively. Probing the cgs$\rightarrow X^0$ resonance, we measure the population inversion ($N_{1X} - N_{cgs}$). The solid lines in Fig. 3(c) show the results of a fit of the photocurrent data to this model with the tunneling rates R_e and R_h and the overall signal amplitude as fitting parameters. We note that this process implicitly assumes an identical oscillator strength for all three probed transitions, an assumption that is in good agreement with time-resolved luminescence measurements that reveal similar radiative lifetimes of X^0 and the negatively ($2X^-$) and positively charge trions (X^+).[26] This relatively simple model produces very good quantitative agreement with the experimental data and allows us to extract an initial X^0 occupation of $N_0=0.65$ as well as tunneling times of $1/R_e=80$ ps for the electron and $1/R_h=148$ ps for the hole. Surprisingly, these findings point toward very fast hole tunneling that proceeds over time scales only a factor of two slower than for electrons. In contrast, one-dimensional Wentzel Kramers Brillouin (WKB) modeling of the tunneling escape rates of electrons from the dot[20] has been successfully used to describe the tunnel rates for electrons while hole tunneling is predicted to be several orders of magnitude slower due to the larger effective mass. The observations discussed here demonstrate that this is not the case, hole tunneling escape proceeding over similar time scales. The main difficulty performing realistic WKB-type calculations lies with the effective height of the tunnel barriers and the value of the carrier effective mass in the highly strained QD barrier material. These parameters are determined by the details of the composition and strain in the dot and small variations drastically change the computed carrier tunnel rates. Furthermore, the Coulomb binding energy of the exciton plays a crucial role since this energy is effectively released after the first tunneling event has occurred, the tunnel barrier of the hole is reduced in both width and height after the electron has left the QD. Assuming a Coulomb energy shift of 20 meV and setting the model parameters used in Ref. 20 to reasonable values the observed fast tunneling rates for electrons and holes are not inconsistent with such WKB models.

V. STRONG EXCITATION PHENOMENA: OPTICAL GAIN, RABI OSCILLATIONS, SINGLE-PULSE BIEXCITON GENERATION

From the discussion of the data in Fig. 3 it has already become evident that a partial population inversion $N_0>0.5$ can be achieved under our experimental conditions. Ideally, pumping the cgs$\rightarrow X^0$ transition with a π pulse, one would expect deterministic single exciton generation, i.e., $N_0=1$. Among other interesting phenomena such a situation would give rise to single-photon gain of a probe pulse tuned to the resonance. We therefore strove to identify pulse parameters where gain is directly visible in photocurrent spectroscopy. Photocurrent results with the largest optical gain achievable in our approach are presented in Fig. 4(a). The red curve

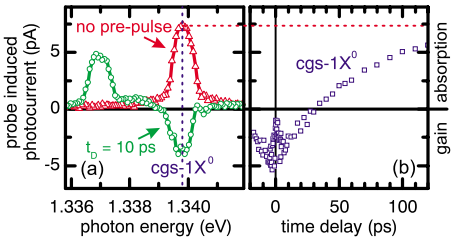

FIG. 4. (Color online) Optical gain for intense excitation: (a) spectral scan of the probe-induced photocurrent for the dot in the cgs (red) and $t_D=10$ ps after excitation with a cgs$\rightarrow X^0$ pump pulse (green). Pump and probe pulse areas are close to π pulses. (b) Temporal scan of the cgs$\rightarrow X^0$ transition. The scattered data points around $t_D=0$ originate from an interference of pump and probe fields.

shows the photocurrent spectrum of the empty QD (blocked pump pulse) with a maximum current amplitude of 7.4 pA. The green curve in Fig. 4(a) shows the photocurrent spectrum obtained $t_D=10$ ps after resonant excitation at cgs$\rightarrow X^0$ with a pump intensity chosen to maximize the negative signal at the excitonic resonance.[27] In this regime the high power pump pulse largely inverts the cgs-X^0 two-level system and stimulated emission into the probe pulse dominates over its absorption. Therefore the overall impact of the probe is to depopulate the X^0 level and our lock-in detection suggests a negative probe-induced photocurrent which is a clear piece of evidence for optical gain. Interestingly, for the maximum gain observed in Fig. 4(a), $\approx$55% of the probe pulses experience a deterministic gain of a single photon. In Fig. 4(b) we show the probe-induced photocurrent for various delay times after pumping the excitonic resonance. The dynamics of the signal follows the model for carrier tunneling developed in Sec. III. Gain is found to persist for time scales longer than 30 ps. After that period, carrier tunneling depopulates the X^0 level such that the probe absorption again outweighs any stimulated emission. We note that an inversion of the cgs-X^0 system by pumping higher levels of the QD as seen by Sotier *et al.*[28] is not observed here. The reason is most probably related to small tunnel barriers from *p*- and *d*-shell levels that depopulate the QD more efficiently than relaxation to the electron and hole ground states.

It is also interesting to detect single-pulse photocurrent spectra for high pulse intensities. Results obtained close to the cgs$\rightarrow X^0$ transition for numerous intensities are presented in Fig. 5. For a relative intensity of 1.2 we observe a photocurrent spectrum similar to the red curve in Fig. 4(a). We note that for this set of experiments the bias voltage to the device is 1 V and, therefore, the resonances are typically shifted by $\approx$1 meV compared to the data presented in Figs. 2 and 4. For larger excitation intensities, the current amplitude at the cgs$\rightarrow X^0$ resonance is seen to saturate or even decay while another absorption peak emerges at a photon energy of 1.3378 eV. Those two absorption lines are analyzed in more detail in panels (b) and (c) of Fig. 5. The results of a power variation in a pulse tuned to the cgs$\rightarrow X^0$ transition are presented in Fig. 5(c), choosing the same power scale as Figs. 5(a) and 5(b) to facilitate direct

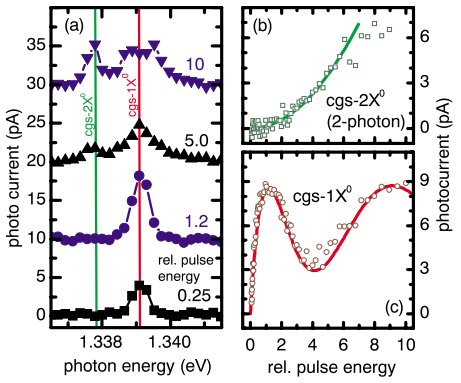

FIG. 5. (Color online) (a) Photocurrent spectra close to the cgs$\rightarrow$X^0 transition for various relative incident powers given in the graph. The spectra are shifted by 10 pA for visibility. (b) Squares: photocurrent detected with a central photon energy of 1.3378 eV, i.e., the mean value of the cgs$\rightarrow$X^0 and the X$^0\rightarrow$2X^0 transition energies. The solid line is a quadratic fit to the data. (c) Photocurrent amplitude detected at the cgs$\rightarrow$X^0 resonance as a function of the relative pulse intensity. Squares are measured current values. The solid line corresponds to a simulation using the Rabi oscillation model described in the text.

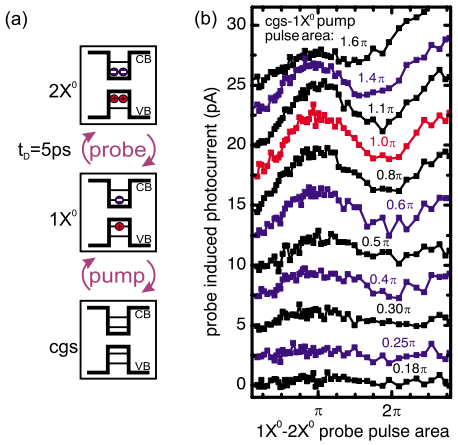

FIG. 6. (Color online) Photocurrent detection of probe-induced Rabi oscillations of the X$^0\rightarrow$2X^0 transition probed 5 ps after pumping the cgs$\rightarrow$X^0 transition. (a) Optically driven transitions between QD states shown in single-particle energy diagrams. (b) Results of probe power scans shown for different powers of the pump pulse. For better visibility the scans are shifted in steps of 2.5 pA along the ordinate.

comparison. The power dependence shows the characteristic behavior of Rabi oscillations as previously observed by several other groups.[8,9,29] From this measurement the power of a π pulse can be read to calibrate the power axis. This proves to be very useful since the near-field amplitude of laser light at the QD position is practically inaccessible by other experimental methods. To model the Rabi oscillation excitation of the cgs-X^0 transition we numerically integrate the Bloch equations for the two-level system interacting with a Gaussian light pulse. Relaxation is described by longitudinal (T_1) and transverse (T_2) relaxation times

$$\frac{1}{T_1} = \frac{1}{T_{tu}} + \frac{1}{T_{sp}}, \tag{5}$$

$$\frac{1}{T_2} = \frac{1}{2T_1} + \frac{1}{T_{pd}}, \tag{6}$$

where T_{tu} is the tunnel lifetime of the carriers. Time-dependent measurements such as those shown in Fig. 3 indicate T_{tu}=18 ps at a bias voltage of 1.0 V used here. The spontaneous emission T_{sp} is set to T_{sp}=0.5 ns and has only minor influence on the simulation results as long as $T_{sp} \gg T_{tu}$. The time constant T_{pd} is related to pure dephasing. Our experiment essentially operates in a regime where T_{tu} is only a factor of six longer than the duration t_P of the driving pulse; so tunneling during the interaction leads to an additional background signal of incoherent absorption. In the simulation, the total photocurrent is computed by integrating the rate of tunnel events from the time-dependent population inversion of the cgs-X^0 system. The solid line in Fig. 5(c) is obtained with a pulse duration t_P=3.3 ps consistent with the bandwidth of the exciting laser pulse. The pure dephasing time is set to T_{pd}=14 ps while the dipole matrix element is adjusted to reproduce the experimental position of maximum photocurrent. The result of the simulation agrees well with the experiment.

We now turn to the photocurrent induced at a photon energy of 1.3378 eV, i.e., the mean value of the cgs$\rightarrow$X^0 and the X$^0\rightarrow$2X^0 transition energies. As seen in Fig. 5(b), the power dependence of the photocurrent amplitude of this resonance is approximately quadratic. We attribute this observation as evidence for direct photoexcitation of the 2X^0 two photon nonlinearity as first observed by Brunner *et al.*[30] and subsequently studied by Stufler *et al.*[31]

VI. CONDITIONAL EXCITON-BIEXCITON RABI OSCILLATIONS

In the final section, we describe how our methods can be used to induce and probe conditional coherent response from the QD. In particular, we focus on the *coherent* dynamics of the induced 2X^0 transition discussed above in relation to Figs. 2 and 3. For these experiments, the pump pulse is tuned resonant to the cgs$\rightarrow$X^0 transition while the subsequently applied probe pulse tests the induced X$^0\rightarrow$2X^0 absorption [see Fig. 6(a)]. Then, both the powers of pump and probe pulse are varied independently and the resulting amplitude of the photocurrent signal is tested. Probe power scans are presented in Fig. 6(b) for different values of the pump pulse area. As already shown in Fig. 5 the pump pulse drives Rabi oscillations between the cgs and X^0 with the commensurate oscillation of the amplitude of the X$^0\rightarrow$2X^0 signal. Most interestingly also the probe pulse drives Rabi oscillations but in the X$^0\leftrightarrow$2X^0 two-level system as can be seen by the oscillatory dependence on probe pulse power. We emphasize that the pump pulse can completely switch on and off this Rabi oscillation induced by the probe pulse. In the situation, when pump and probe pulses are both π pulses (in the maximum of the curve for pump pulse area 1.0 π in Fig. 6), the QD is prepared in a 2X^0 state and the sample acts as deter-

ministic source of current delivering two electrons per excitation cycle. In the language of quantum information processing, the results shown in Fig. 6 represent the QD implementation of a conditional ROT gate (CROT).[13] We note, however, that the maximum observed probe-induced photocurrent of 5 pA suggests a limited fidelity of the CROT operation. More detailed studies involving the choice of lower bias voltage, different pump/probe pulse bandwidths and timing delays would be required to optimize the CROT functionality.

VII. CONCLUSION

In conclusion we have demonstrated picosecond pump-probe style experiments on a single QD taking advantage of sensitive photocurrent readout. Creating an exciton in the QD with a pump pulse, spectroscopic lines of the biexciton, not only in its ground state but also of excited biexciton states, have been identified. From time-resolved measurements the tunneling time of electrons and holes from the quantum dot to the sample contacts could be measured. That way, hole tunneling was found to be unexpectedly fast. At high pulse powers single-pulse two-photon generation of biexcitons was observed. Finally exciton Rabi oscillations and conditional biexciton Rabi oscillations were demonstrated.

ACKNOWLEDGMENTS

The authors would like to thank H. Krenner for valuable discussions. This work is supported by the DFG in the framework of the Sonderforschungsbereich SFB631.

*mzecherle ph.tum.de

[1] A. Zrenner, J. Chem. Phys. **112**, 7790 (2000).
[2] A. Yoffe, Adv. Phys. **50**, 1 (2001).
[3] M. Skolnick and D. Mowbray, Annu. Rev. Mater. Res. **34**, 181 (2004).
[4] Y. Arakawa and H. Sakaki, Appl. Phys. Lett. **40**, 939 (1982).
[5] P. Bhattacharya, Z. Mi, J. Yang, D. Basu, and D. Saha, J. Cryst. Growth **311**, 1625 (2009).
[6] F. Troiani, U. Hohenester, and E. Molinari, Phys. Rev. B **62**, R2263 (2000).
[7] N. Bonadeo, J. Erland, D. Gammon, D. Park, D. Katzer, and D. Steel, Science **282**, 1473 (1998).
[8] A. Zrenner, E. Beham, S. Stufler, F. Findeis, M. Bichler, and G. Abstreiter, Nature (London) **418**, 612 (2002).
[9] T. H. Stievater, X. Li, D. G. Steel, D. Gammon, D. S. Katzer, D. Park, C. Piermarocchi, and L. J. Sham, Phys. Rev. Lett. **87**, 133603 (2001).
[10] T. Unold, K. Mueller, C. Lienau, T. Elsaesser, and A. D. Wieck, Phys. Rev. Lett. **94**, 137404 (2005).
[11] S. Stufler, P. Ester, A. Zrenner, and M. Bichler, Phys. Rev. Lett. **96**, 037402 (2006).
[12] X. Li, Y. Wu, D. Steel, D. Gammon, T. Stievater, D. Katzer, D. Park, C. Piermarocchi, and L. Sham, Science **301**, 809 (2003).
[13] S. J. Boyle, A. J. Ramsay, F. Bello, H. Y. Liu, M. Hopkinson, A. M. Fox, and M. S. Skolnick, Phys. Rev. B **78**, 075301 (2008).
[14] S. J. Boyle, A. J. Ramsay, A. M. Fox, M. S. Skolnick, A. P. Heberle, and M. Hopkinson, Phys. Rev. Lett. **102**, 207401 (2009).
[15] P. W. Fry, J. J. Finley, L. Wilson, A. Lemaitre, D. Mowbray, M. Skolnick, M. Hopkinson, G. Hill, and J. Clark, Appl. Phys. Lett. **77**, 4344 (2000).
[16] C. Ruppert and M. Betz, Opt. Express **16**, 5572 (2008).
[17] R. Grote and H. Fouckhardt, Opt. Express **4**, 328 (1999).
[18] P. W. Fry, I. E. Itskevich, D. J. Mowbray, M. S. Skolnick, J. J. Finley, J. A. Barker, E. P. O'Reilly, L. R. Wilson, I. A. Larkin, P. A. Maksym, M. Hopkinson, M. Al-Khafaji, J. P. R. David, A. G. Cullis, G. Hill, and J. C. Clark, Phys. Rev. Lett. **84**, 733 (2000).
[19] F. Findeis, M. Baier, E. Beham, A. Zrenner, and G. Abstreiter, Appl. Phys. Lett. **78**, 2958 (2001).
[20] P. W. Fry, I. E. Itskevich, S. R. Parnell, J. J. Finley, L. R. Wilson, K. L. Schumacher, D. J. Mowbray, M. S. Skolnick, M. Al-Khafaji, A. G. Cullis, M. Hopkinson, J. C. Clark, and G. Hill, Phys. Rev. B **62**, 16784 (2000).
[21] S. Stufler, P. Ester, A. Zrenner, and M. Bichler, Phys. Rev. B **72**, 121301(R) (2005).
[22] S. Schmitt-Rink, D. A. B. Miller, and D. S. Chemla, Phys. Rev. B **35**, 8113 (1987).
[23] B. Adolph, S. Glutsch, and F. Bechstedt, Phys. Rev. B **48**, 15077 (1993).
[24] U. Bockelmann, K. Brunner, and G. Abstreiter, Solid-State Electron. **37**, 1109 (1994).
[25] V. Mlinar and A. Zunger, Phys. Rev. B **80**, 205311 (2009).
[26] M. Kaniber, A. Laucht, A. Neumann, J. M. Villas-Bôas, M. Bichler, M.-C. Amann, and J. J. Finley, Phys. Rev. B **77**, 161303 (2008).
[27] The corresponding pulse energy of 2.2 fJ per pulse is close to the one which will be referred to as π pulse later in Sec. V.
[28] F. Sotier, T. Thomay, T. Hanke, J. Korger, S. Mahapatra, A. Frey, K. Brunner, R. Bratschitsch, and A. Leitenstorfer, Nat. Phys. **5**, 352 (2009).
[29] H. Kamada, H. Gotoh, J. Temmyo, T. Takagahara, and H. Ando, Phys. Rev. Lett. **87**, 246401 (2001).
[30] K. Brunner, G. Abstreiter, G. Böhm, G. Tränkle, and G. Weimann, Phys. Rev. Lett. **73**, 1138 (1994).
[31] S. Stufler, P. Machnikowski, P. Ester, M. Bichler, V. M. Axt, T. Kuhn, and A. Zrenner, Phys. Rev. B **73**, 125304 (2006).